



Low-temperature solution processing of palladium/palladium oxide films and their pH sensing performance



Yiheng Qin ^{a,b}, Arif U. Alam ^a, Si Pan ^c, Matiar M.R. Howlader ^{a,*}, Raja Ghosh ^c, P. Ravi Selvaganapathy ^d, Yiliang Wu ^{b,**}, M. Jamal Deen ^{a,*}

^a Department of Electrical and Computer Engineering, McMaster University, 1280 Main Street West, Hamilton, ON, Canada L8S 4K1

^b Advanced Materials Laboratory, Xerox Research Centre of Canada, 2660 Speakman Drive, Mississauga, ON, Canada L5K 2L1

^c Department of Chemical Engineering, McMaster University, 1280 Main Street West, Hamilton, ON, Canada L8S 4L7

^d Department of Mechanical Engineering, McMaster University, 1280 Main Street West, Hamilton, ON, Canada L8S 4L7

ARTICLE INFO

Article history:

Received 24 June 2015

Received in revised form

26 August 2015

Accepted 27 August 2015

Available online 11 September 2015

Keywords:

PH sensor

Potentiometric sensing

Palladium oxide

Solution processing

Low-temperature

ABSTRACT

Highly sensitive, easy-to-fabricate, and low-cost pH sensors with small dimensions are required to monitor human bodily fluids, drinking water quality and chemical/biological processes. In this study, a low-temperature, solution-based process is developed to prepare palladium/palladium oxide (Pd/PdO) thin films for pH sensing. A precursor solution for Pd is spin coated onto pre-cleaned glass substrates and annealed at low temperature to generate Pd and PdO. The percentages of PdO at the surface and in the bulk of the electrodes are correlated to their sensing performance, which was studied by using the X-ray photoelectron spectroscope. Large amounts of PdO introduced by prolonged annealing improve the electrode's sensitivity and long-term stability. Atomic force microscopy study showed that the low-temperature annealing results in a smooth electrode surface, which contributes to a fast response. Nano-voids at the electrode surfaces were observed by scanning electron microscope, indicating a reason for the long-term degradation of the pH sensitivity. Using the optimized annealing parameters of 200 °C for 48 h, a linear pH response with sensitivity of 64.71 ± 0.56 mV/pH is obtained for pH between 2 and 12. These electrodes show a response time shorter than 18 s, hysteresis less than 8 mV and stability over 60 days. High reproducibility in the sensing performance is achieved. This low-temperature solution-processed sensing electrode shows the potential for the development of pH sensing systems on flexible substrates over a large area at low cost without using vacuum equipment.

© 2015 Elsevier B.V. All rights reserved.

1. Introduction

pH sensors are of significant importance for *in vivo* monitoring of bodily fluids [1] and online monitoring of water quality [2]. Since conventional glass pH electrodes are fragile, large in dimensions, difficult to handle, and require frequent calibration and maintenance [3], it is challenging to apply them in confined spaces for continuous use in many health and environmental monitoring applications. Therefore, small-size, flexible, easy-to-use, and low-cost pH sensors with sensitive and reliable performance are needed. Among the various types of pH sensors that include chemical-mechanical sensors, optical sensors, ion-sensitive field-effect

transistor-based sensors, and resistor-based sensors [4], the potentiometric sensor is one of the most commonly studied configurations owing to its straightforward and compact structure, potential for miniaturization, ease in fabrication and integration, low power consumption, as well as compatibility with both organic and inorganic materials.

The pH sensing behavior of a number of metal oxides have been studied for potentiometric sensors. For example, copper oxide [5], iridium oxide (IrO_x) [6–9], cobalt oxide [10], tungsten oxide [11,12], ruthenium oxide [13], titanium oxide (TiO₂) [14], zinc oxide (ZnO) [15], palladium oxide (PdO) [16], and lead oxide [17] have been used in pH sensors. Among these materials, PdO is highly promising because of its demonstrated higher (super-Nernstian) sensitivity than that of many materials. Also, it has fast response (< 10 s) in a wide sensing range of pH between 2 and 12, and long lifetime (up to several years) [18–21]. However, the fabrication of high-quality PdO films at low temperature and low cost is challenging.

* Corresponding authors.

** Corresponding author. Present address: TE Connectivity, 306 Constitution Drive, Menlo Park, CA 94025, USA

E-mail addresses: mrhowlader@ece.mcmaster.ca (M.M.R. Howlader), yiliangwu@hotmail.com (Y. Wu), jamal@mcmaster.ca (M.J. Deen).

Currently, thermal oxidation [19,22], physical vapor deposition [21,23,24] and electrochemical deposition [18,25,26] are being used to fabricate Pd/PdO films. In these processes, the challenges are the requirements of high temperatures (above 400 °C), vacuum environment and high electrical energy. Moreover, it is challenging to pattern electrodes on electrochemically deposited films because of the requirements of masks and additional lithographic steps [6,8,9,27]. These process conditions are incompatible with the development of cost-effective pH sensors on inexpensive polymeric substrates [28], as well as their integration with electronics for sensing systems [29,30]. Thus, alternative approaches for material deposition such as low-temperature solution processing have to be employed. Earlier, screen-printed Pd has been investigated for electrochemical sensing [31]. The fabricated electrodes were porous and contained PdO, but they were not pH sensitive. On the other hand, while solution-processed IrO_x [32], TiO₂ [33] and ZnO [34] have been reported for pH sensors, so far, PdO-based pH sensing electrodes have not yet been prepared from solution.

In this study, we fabricated Pd/PdO pH sensing electrodes using a simple, low-temperature, and low-cost solution-based process. Pd precursor solution was spin coated onto glass substrates, followed by annealing in ambient air at low temperatures. The annealing process converted organic Pd complex to metallic Pd and further oxidized Pd to PdO. We optimized the processing parameters and characterized the fabricated Pd/PdO films to achieve high quality of sensing electrodes. Potentiometric measurements were used to characterize the pH sensing performance of the electrodes. Also, we investigated their reproducibility and long-term stability. Finally, we proposed the compatibility of the solution-based process for large-area manufacturing on polymeric substrates for cost-effective pH sensors.

2. Experimental section

2.1. Fabrication of pH sensing electrodes

The glass substrates (7525 M, J. Melvin Freed Brand microscope slides) were manually cut into 1 in. × 1.5 in. pieces using a diamond scribe, followed by rinsing with isopropanol (≥ 99.5%, ACS reagent grade, 8600-1, Caledon Laboratory Chemicals) and deionized water, and then dried under compressed dry air. Commercially available Pd precursor solution (Pd-25c) was obtained from Xerox Research Centre of Canada and used without further purification. This clear light-yellow solution has a metal content ~10 wt% with a decomposition temperature of ~190 °C. About 0.5 mL of the Pd precursor solution was dispensed onto glass substrates using a pipette and left settling for 2 min before spin coating. The coating was performed at 500 rpm for 10 s with 800 rpm/s acceleration and subsequently 3000 rpm for 60 s with 800 rpm/s acceleration. Then, the samples were baked on a hot-plate, in ambient air, at different temperatures (200 °C and 250 °C) and for different durations (4 min, 24 h, and 48 h). After annealing, the electrodes were characterized. The area of the sensing electrode was ~9.6 cm², but it could be miniaturized using patterning techniques.

2.2. Characterization of pH sensing electrodes

The thickness of the Pd/PdO layers was measured by using a stylus profiler (Dektak XT, Bruker). A pair of stainless steel tweezers was used to gently scratch the deposited thin films to expose the glass substrates. The stylus was scanned at a speed of 50 μm/s between the exposed glass and Pd/PdO with 3 mg applied force. X-ray photoelectron spectroscopy (XPS, JPS-9200, JEOL) was used

to analyze the chemical composition of sensing electrodes. Narrow-scan spectra (resolution of 0.1 eV) were obtained using a magnesium X-ray source (10 keV and 15 mA). Depth profiling spectra were acquired after every 40 s of argon (Ar) ion etching (3 keV and 20 mA) at a pressure of 0.08 Pa. Four etching steps were carried out at one analysis location. XPSPEAK 4.1 software was used for curve fitting and to calculate the area under peaks to determine the films' chemical composition. Atomic force microscopy (AFM, Dimension Icon, Bruker) was used to measure the surface roughness of the sensing electrodes. The AFM measurements were based on tapping mode with 20 μm × 20 μm and 1 μm × 1 μm scanning areas using a 1 Hz scanning rate. The surface roughness was calculated using NanoScope Analysis software. A field-emission scanning electron microscopy (SEM, SU-8000, Hitachi) operating in deceleration mode with a landing voltage of 700 V was used to observe the surfaces of Pd/PdO sensing films.

2.3. pH sensing test

Britton–Robinson pH buffer solutions (pH=2, 4, 6, 8, 10, and 12) were prepared by mixing an acid solution comprising 0.04 M phosphoric acid (≥ 85 wt%, ACS reagent grade, 695017, Sigma-Aldrich), 0.04 M acetic acid (≥ 99.7%, ACS reagent grade, 1000-1, Caledon Laboratory Chemicals), 0.04 M boric acid (99.97%, 339067, Sigma-Aldrich) with an appropriate amount of 0.2 M sodium hydroxide (≥ 98%, ACS reagent grade, S5881, Sigma-Aldrich) solution. The pH levels of buffer solutions were monitored by a commercial pH meter (PHB-600R, OMEGA) with a glass electrode (PHE1311, OMEGA) during preparation. The pH sensing performance of the fabricated electrodes was characterized based on a potentiometric configuration against a silver/silver chloride (Ag/AgCl) reference electrode (CHI111, CH Instruments). The bottom half of the sensing electrode and reference electrode (~2 cm distance between them) was immersed in static pH buffer solutions at the same time and connected to a Keithley 4200-SCS semiconductor analyzer using alligator clamps. The semiconductor analyzer was set for measuring the open circuit voltage by forcing the current flowing through the sensing and reference electrodes to be 0 A with a “Best Fixed” source range. This setting resulted a voltage sampling interval of ~6 s. The deposited Pd/PdO was used for the dual purpose of sensing as well as electrical contact because it was electrically conductive. The open circuit potential between the sensing and reference electrode was recorded as a function of time at room temperature (23 ± 2 °C). The sensing electrodes were tested in each pH buffer for about 80 s and immediately transferred into the next pH buffer without rinsing (with deionized water) or drying. To study the operation stability, the sensing electrodes were tested multiple times over a 60-day period. For the storage stability, the pH sensing electrodes were kept in ambient air at room temperature for 60 days before pH sensing measurements.

3. Results and discussions

3.1. Solution processing of Pd/PdO electrodes

The fabrication of pH sensing electrodes was straightforward, including spin coating and annealing in ambient air. The annealing temperature of 200 °C was decided based on two reasons. First, such temperature should be higher than the decomposition temperature of the Pd precursor (~190 °C). Second, a low annealing temperature is preferred to allow the precursor being processed on a wider range of substrates (including low-cost polymeric substrates). The annealing included 2 steps: a short-term conversion step and a long-term oxidation step. In the conversion step,

Table 1

Summary of preparation conditions, thickness, chemical composition, and performance parameters of pH sensing electrodes.

Sample ID	Annealing temperature (°C)	Annealing time	Thickness (nm)	PdO% at the surface (%)	PdO% in the bulk (%)	pH sensitivity (mV/pH)	Linearity ^a
A	200	4 min	85.7 ± 4.9	51	18	54.53 ± 1.70	0.9988
B	200	24 h	121.3 ± 7.2	82	47	68.93 ± 1.74	0.9995
C	200	48 h	125.1 ± 5.9	98	49	64.71 ± 0.56	0.9991
D	250	4 min	93.6 ± 5.3	89	26	65.64 ± 1.46	0.9996
E	250	24 h	125.0 ± 6.2	97	49	64.62 ± 1.65	0.9993
F	250	48 h	125.3 ± 4.0	99	53	63.19 ± 1.47	0.9994

^a Linearity is compared using the correlation coefficient R^2 .

the clear light-yellow precursor solution turned to black color within 1 min upon heating, indicating the decomposition of the precursor and the formation of Pd nanoparticles. After annealing for another 1–2 min, metallic silver color appeared because of the agglomeration of Pd nanoparticles to a thin film. Since the conversion was performed in air, a certain amount of PdO was

produced in this step. In addition, good adhesion between the deposited Pd/PdO thin films and glass substrate were confirmed by scotch tape test.

To study the effect of PdO percentage on the pH sensing behavior, the samples were annealed in air for 4 min, 24 h, and 48 h at 200 °C. Another conversion and annealing temperature (250 °C)

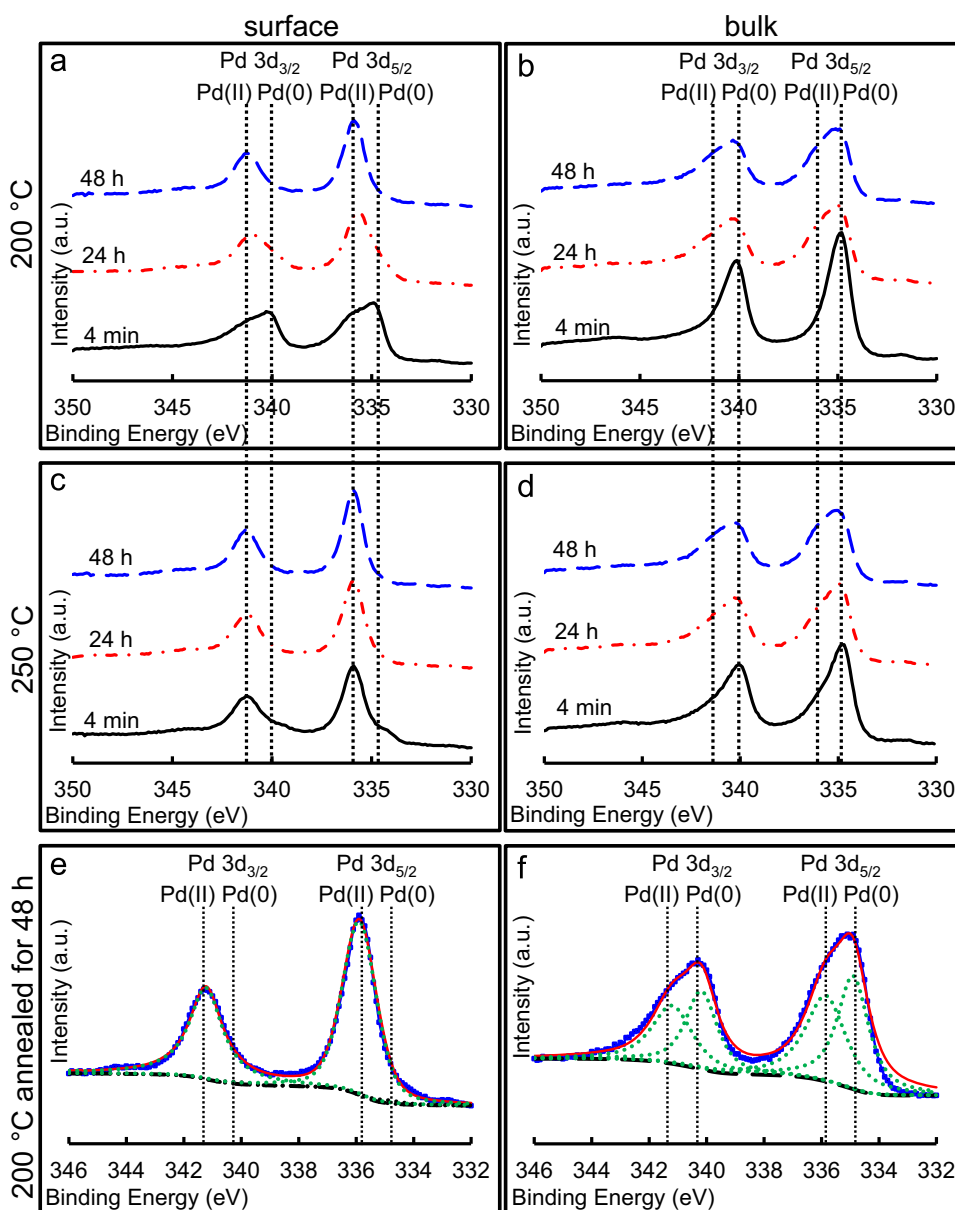


Fig. 1. (a)–(d) Pd 3d XPS spectra of the surface and bulk of sensing electrodes annealed at different temperatures for 4 min (solid lines), 24 h (dot-dash lines), and 48 h (dashed lines). (a) Surface, 200 °C. (b) Bulk, 200 °C. (c) Surface, 250 °C. (d) Bulk, 250 °C. (e) and (f) Curve fitting of XPS spectra for calculating atomic ratio between Pd(0) and Pd(II); square boxes are original data, solid lines are fitted curves, dotted lines are fitted peaks for Pd(0) and Pd(II), and dashed lines are background lines. (e) Surface of a sample annealed at 200 °C for 48 h (the intensity of 2 Pd(0) peaks is too low to be seen). (f) Bulk of the same sample annealed at 200 °C for 48 h.

was used to accelerate the generation of PdO for 4 min, 24 h, and 48 h. In total, 6 groups of samples (A–F) were prepared and are listed in Table 1. The average thickness (taken over 5 locations) of a sample annealed at 200 °C for 4 min was 85.7 nm. The Pd/PdO thin films became thicker if a higher annealing temperature or a longer annealing time was used. The increased thickness was attributed to the volume expansion induced by the generation of PdO.

3.2. Characterization of Pd/PdO thin films

3.2.1. Chemical compositions

The chemical composition at the surface and in the bulk of deposited Pd/PdO electrodes was characterized by XPS. XPS spectra for the surface were obtained without Ar ion etching while those for the bulk were got after 160 s of etching (etch rate ~0.44 nm/s, XPS spectra after 40 s of etching are identical at each location for analysis). Fig. 1(a)–(d) shows XPS spectra of Pd 3d region for the surface and bulk of sensing electrodes annealed at 6 different conditions.

For the surface of the electrode prepared at 200 °C for 4 min (sample A), peaks for Pd 3d_{5/2} and Pd 3d_{3/2} doublet were at binding energies around 334.90 eV and 340.22 eV, respectively (Fig. 1(a), solid line). These peak positions indicate the presence of metallic Pd (Pd(0)) [35,36]. Noteworthy, shoulders could be observed on the left side (high-energy side) of Pd(0) peaks, which suggests the existence of Pd(II) because PdO has been considered as a stable oxide form of Pd [37]. In the bulk of the same sample (Fig. 1(b), solid line), peaks for Pd 3d_{5/2} and Pd 3d_{3/2} do not shift, but the shoulders are less obvious, designating a smaller amount of Pd(II).

Next, we studied the effects of annealing on the film properties. With increasing annealing times, peaks for Pd 3d_{5/2} and Pd 3d_{3/2} shift to higher binding energies for both surface and bulk spectra. This shift can be explained by the increased amount of Pd(II). For the sample annealed at 250 °C for 4 min (sample D, Fig. 1(c), solid line), Pd(II) is the major surface composition because peaks for Pd 3d_{5/2} and Pd 3d_{3/2} have higher binding energies than the sample annealed at 200 °C for 4 min. In its bulk spectrum (Fig. 1(d), solid line), we can also observe a significant amount of Pd(II). Longer annealing time at 250 °C slightly shifts the peaks to the high-energy side (sample E and F, Fig. 1(c) and (d), dot-dash and dashed lines), which means the amount of Pd(II) gradually reaches saturation.

To quantitatively find the atomic percentage of Pd(II), the XPS spectra of Pd 3d doublet were fitted using 4 peaks (each of Pd 3d_{3/2} and Pd 3d_{5/2} was fitted by one Pd(0) and one Pd(II) peak). Fig. 1(e) and (f) shows the curve fitting of the surface and bulk spectra of the sample annealed at 200 °C for 48 h (sample C). The atomic percentage of Pd(II) (also the percentage of PdO) for all types of electrodes is calculated and listed in Table 1. At the beginning of annealing, the amount of PdO at the surface and in the bulk increased quickly (compare sample A and D with B and E), since oxygen (O₂) in air diffused into the film and reacted with metallic Pd. Later, it was more difficult for O₂ to diffuse into the film because the surface became denser. Therefore, the difference in PdO% between the 48 h-annealed and 24 h-annealed samples was not significant (compare sample B and E with C and F). Besides, the time for PdO formation can be shortened by using higher annealing temperature, or annealing in an oxidation atmosphere, such as in O₂.

3.2.2. Surface morphologies

Fig. 2 shows AFM images that illustrate the surface roughness of sensing electrodes prepared at different temperatures. Similar roughness values were obtained on samples annealed at the same temperature for different durations. When the precursor was

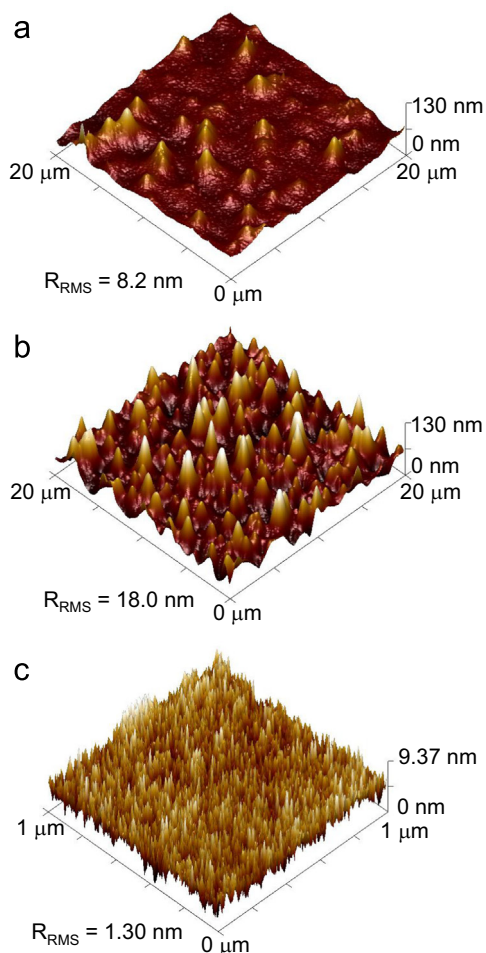


Fig. 2. (a) and (b) AFM images over a 20 μm × 20 μm area of surfaces of pH sensing electrodes annealed at (a) 200 °C and (b) 250 °C for 48 h. (c) AFM image over a 1 μm × 1 μm area of surfaces of a pH sensing electrode annealed at 200 °C for 48 h.

converted to Pd at 200 °C, the nucleation and coalescence of generated Pd/PdO nanoparticles, together with the decomposition of organic compounds, introduced peaks and valleys in the deposited film [38]. The resulting surface roughness for the electrodes annealed at 200 °C had a root-mean-square (RMS) value of 8.1 ± 1.1 nm over a 20 μm × 20 μm area (3 measurements were done on each sample). Fig. 2(a) shows an example of an electrode annealed at 200 °C for 48 h. Its RMS roughness was 8.2 nm. Elevating the conversion temperature to 250 °C resulted in a faster solvent evaporation. Thus, agglomerates with smaller sizes were formed, and more peaks/valleys with larger amplitudes were created. The formation of such rough surfaces was due to the fast solvent evaporation, which shortened the time for self-leveling and smoothing of the film [39]. Hence, a higher surface roughness (RMS value of 17.9 ± 3.0 nm) was observed for the electrode annealed at 250 °C. The AFM image of an electrode annealed at 250 °C for 48 h (sample F) is shown in Fig. 2(b). The RMS roughness of the sample was 18.0 nm.

The surface morphology was analyzed in more detail by shrinking the scanning area to 1 μm × 1 μm. Similar AFM images were obtained for the electrodes annealed at all 6 different conditions (RMS roughness was 1.7 ± 0.4 nm). As one example, nanoparticles with diameters around 10 nm were densely packed at the surface of the electrode annealed at 200 °C for 48 h. The RMS value of the surface roughness in this case is 1.30 nm.

SEM observations were done in addition to AFM measurements. Voids of nanoscale dimensions are observed among crystal

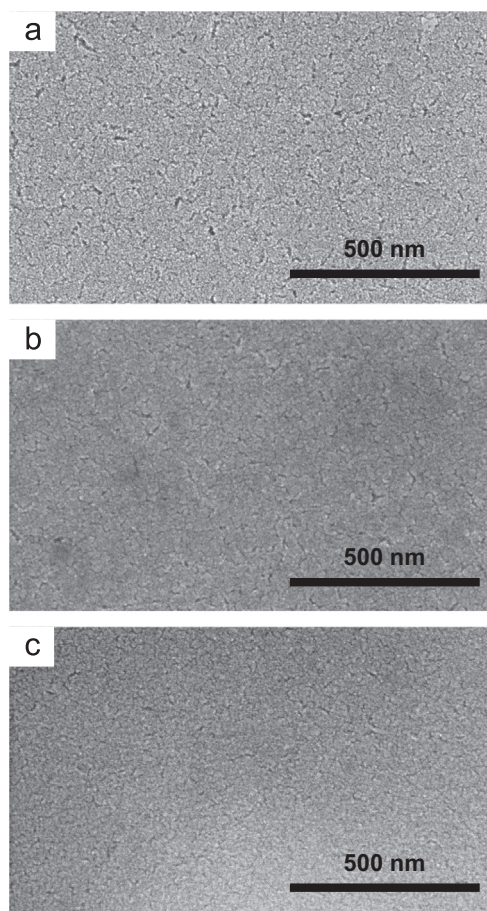
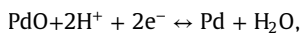


Fig. 3. SEM images of surfaces of sensing electrodes annealed (a) at 200 °C for 4 min, (b) at 200 °C for 48 h, and (c) at 250 °C for 4 min.

domains in all samples. These voids were probably generated by the decomposition of organic compounds in the precursor. Inside the crystal domains, Pd/PdO nanoparticles are closely fused, which agrees with the results from AFM analysis. With an increase of the annealing time from 4 min to 48 h, a less porous film was obtained. Also, the size and amount of nano-voids were reduced (compare Fig. 3(a) with Fig. 3(b)). With an increase of the annealing temperature from 200 °C to 250 °C, a denser film could be obtained as well. Fig. 3(c) is the surface of an electrode annealed at 250 °C for 4 min, which appears to be similar to the surface of the electrode annealed at 200 °C for 48 h. Moreover, annealing time does not affect the surface morphology when annealed at 250 °C (SEM images of other samples are shown in Fig. S2 in supplementary file). Thus, a dense electrode surface with few nano-voids can be produced by increasing annealing time or by elevating annealing temperature.

3.3. pH sensitivity

Even though the pH sensing behavior of Pd/PdO electrodes was studied for many years, the sensing mechanism is still not fully understood [40]. One commonly accepted mechanism depends on the following redox reaction between PdO and Pd:



where every involved hydrogen ion leads to the transfer of one electron. The redox potential can then be described using Nernst equation:

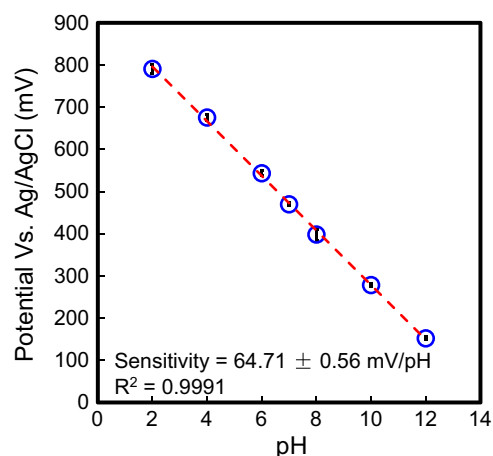


Fig. 4. Open circuit potential versus pH values for an electrode annealed at 200 °C for 48 h (error bars are smaller than the circles as data symbols).

$$E = E^0 - \frac{2.303RT}{F}\text{pH} = E^0 - 0.05916\text{pH},$$

where E^0 is the standard electrode potential, R is the gas constant, T is the absolute temperature, and F is the Faraday constant. At 25 °C, the slope of the ideal potential–pH curve is 59.16 mV/pH, which is the theoretical pH sensitivity.

pH sensing electrodes prepared under 6 different conditions (A–F in Table 1) were characterized potentiometrically by recording the open circuit potential in Britton–Robinson buffer solutions with pH values of 2, 4, 6, 7, 8, 10, and 12. Four consecutive measurement cycles (2 to 12 to 2 to 12 to 2) were performed and the average potential values were plotted versus pH. The plots in Fig. 4 and Fig. S3 were used to determine the pH sensitivity of fabricated electrodes (Fig. 4: the sample annealed at 200 °C for 48 h; Fig. S3: the other 5 types of samples). Sensitivity values calculated from these plots are summarized in Table 1. For the sample annealed at 200 °C for 4 min, a relatively lower sensitivity and linearity was obtained. Such sensing behavior can be attributed to the relatively small fraction of PdO at the electrode surface, where the redox reaction takes place, compared to the samples annealed for longer times or higher temperatures. Although metallic Pd is also sensitive to pH, its sensing mechanism is believed to be different from that of PdO [41]. Metallic Pd exhibited poor sensitivity in basic solutions than in acid solutions, which lowered its sensitivity and linearity over the pH range of 2 to 12 (Fig. S3(a)).

If the samples were annealed at a higher temperature or for a longer time, the electrode surfaces consisted of > 80% PdO and super-Nernstian response (sensitivity higher than 59.16 mV/pH) could be observed, as shown in Table 1. The super-Nernstian behavior of Pd/PdO sensing electrodes was reported previously [18,21], but a detailed explanation for this phenomenon was lacking. We believe that this super-Nernstian behavior of Pd/PdO is similar to that observed in pH sensing electrodes with electrochemically deposited IrO_x . The origin of such super-Nernstian response in IrO_x electrodes was described in detail in reference [6]. We believe that oxides of Pd (PdO_x) and IrO_x may possess similar behavior. It was found that PdO_x can be hydrous [42] and Pd may have higher valence in its oxides (for example, PdO_2) [43]. Hence, the super-Nernstian response of Pd/PdO electrodes may be attributed to the uptake/release of hydrogen ions of hydrous PdO_x without transferring electrons. Therefore, when m electrons and n hydrogen ions ($m < n$) are transferred, the pH sensitivity is enhanced by a factor of n/m according to the Nernst equation. Then the resulting sensitivity can be written as $(n/m)(RT/F) > 59.16$ mV/pH at 25 °C. If more hydrous PdO_x exists in the film, this effect is

more pronounced, and higher sensitivity is expected. The high-resolution XPS spectra did not show visible peaks for Pd with higher valences. This suggests the amount of PdO_x ($x > 1$) is not in the detectable range of the XPS. This result agrees with the pH sensitivity of ~ 65 mV/pH in this study. In addition, the increase of annealing time or annealing temperature decreased the sensitivity slightly (neglect the electrode annealed at 200°C for 4 min). The degradation of the performance might be related to the decomposition of unstable PdO_x ($x > 1$) to PdO [43]. The reduced amount of PdO_x ($x > 1$) limited the reactions between hydrous PdO_x and drove the sensitivity to the theoretical value of 59.16 mV/pH. On the other hand, the anhydrous PdO_x films deposited under many vacuum or high-temperature conditions resulted in lower sensitivity [16,20–24]. In contrast, PdO_x prepared by electrochemical methods had more hydrous oxides and the sensitivity was higher (~ 71 mV/pH) [18] than that in this study (~ 65 mV/pH). Therefore, the super-Nernstian behavior may be related to the hydrous PdO_x ($x > 1$) obtained at low temperatures without using vacuum processing. Further investigation is required to understand the detailed mechanism of the super-Nernstian behavior of the Pd/PdO pH sensing electrodes.

3.4. Response time and reversibility

Response time and reversibility of Pd/PdO sensing electrodes were studied by continuous testing. The electrodes were tested in each pH buffer for about 80 s and immediately transferred into the next pH buffer without rinsing with deionized water or blow drying. The open circuit potential as a function of time for the electrode annealed at 200°C for 48 h is plotted in Fig. 5(a) with an enlarged view in Fig. 5(b) (the real-time pH response of the other 5 types of electrodes are shown in Fig. S4). Smooth transition of the potential signals could be observed. The response time (t_{90} in Fig. 5(b)), which is defined as the time required for 90% change of measured voltage from initial values to final values (ΔV_{90} in Fig. 5(b)), can be extracted from Fig. 5(a).

For our sensing electrodes, the response time was less than 18 s for all pH values, but this response time is longer than the values reported in other studies (less than 2 s) [7,44]. The faster response achieved in these studies relied on smoother and denser electrode surface, which was prepared by high-temperature or high-pressure treatment. These process conditions are not compatible with low-cost, flexible substrates. In our case, this response time of

< 18 s is fast enough for practical use in applications such as on-line water quality monitoring. Also, such relatively slower response may be due to ion diffusion into the nano-voids among Pd/PdO crystal domains (shown in Fig. 3) [5,44,45]. Further, the response was slightly faster in the acid region than in the basic region. This difference was explained in reference [22] as due to some minor reaction (such as the reaction between Pd and hydroxide ions) that happens at the electrode surface. Comparing the electrodes annealed at different temperatures, the response time is shorter when electrodes were annealed at 200°C (< 18 s) than at 250°C (< 30 s) (see Table S1 for the detailed values of response time of different electrodes at various pH levels). This faster response may be related to the smoother electrode surface, which allows faster redox equilibrium between Pd/PdO and hydrogen ions at surface and buried sites [46].

The hysteresis at each pH level was calculated to examine the reversibility behavior of the sensing electrode. For the electrode annealed at 200°C for 48 h, hysteresis less than 7.81 mV (1.24% as the normalized value over the testing pH range) at all pH levels was obtained, indicating that the redox reaction between PdO and hydrogen ion was highly reversible. Furthermore, no apparent correlation was found between annealing conditions and hysteresis characteristics (see Table S2 for detailed values of hysteresis of different electrodes at various pH levels).

3.5. Stability and reproducibility

The stability of pH sensing electrodes is essential for their long-term usage [47–50], and can be categorized into operation stability and storage stability. The operation stability was studied by carrying out pH measurements every few days over a 60-day period. Each pH measurement involved 4 pH cycles (2 to 12 to 2 to 12 to 2) with a measurement time of 80 s at each pH level, after which, the average sensitivity was recorded. The electrodes were stored in ambient air at room temperature without any maintenance or special precaution. The evolution of the sensitivity values for electrodes (annealed at 200°C for 48 h, 250°C for 4 min, and 250°C for 48 h) up to 60 days is plotted in Fig. 6.

For all monitored electrodes, a decrease in sensitivity values was observed. The sensitivity of the electrode annealed at 250°C for 4 min showed a fast decreasing, while the sensitivity degradation of the other 2 electrodes was much slower. Linear fitting of the scattered data was used to calculate the degradation rate of

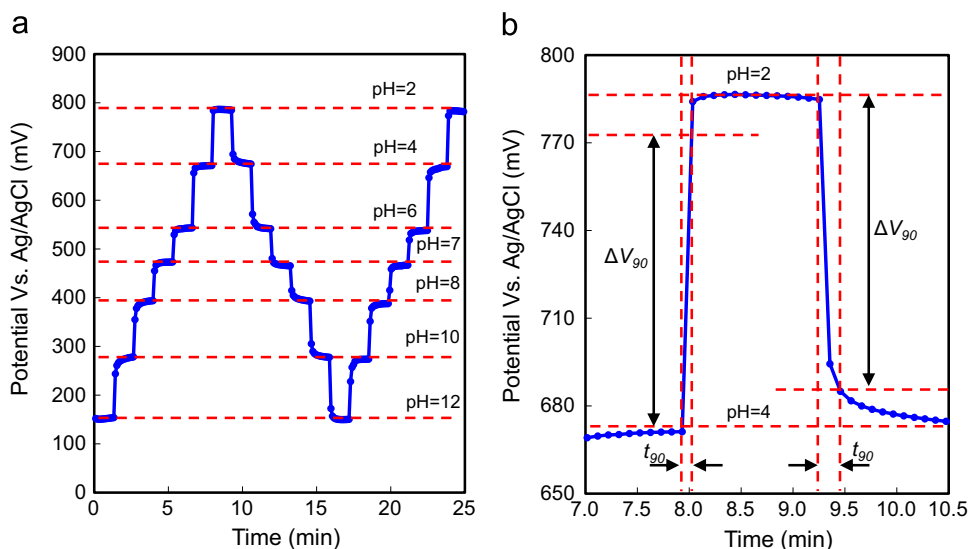


Fig. 5. Real-time response of an electrode annealed at 200°C for 48 h between pH of 2 and 12. (a) Full-scale view. (b) Enlarged view of the voltage transition between pH=2 and 4, indicating how the response time was determined.

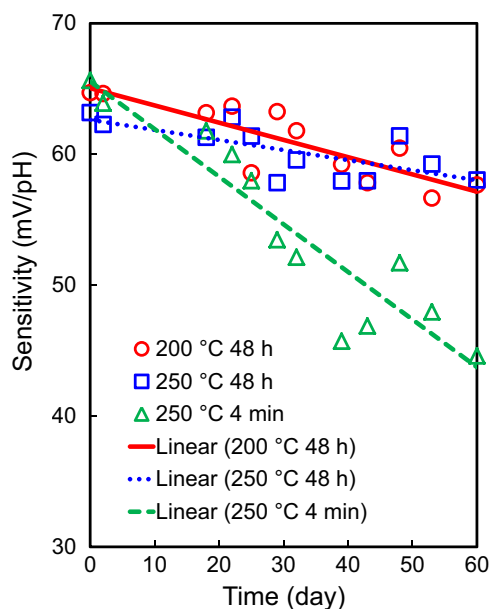


Fig. 6. Operation stability of Pd/PdO pH sensing electrodes over a 60-day period.

sensitivity, which was -0.36 mV/pH/day for the electrode annealed at 250 °C for 4 min. Electrodes annealed at 200 °C and 250 °C for 48 h exhibited a slow degradation rate (-0.13 , and -0.08 mV/pH/day, respectively). In addition, both electrodes still maintained near-Nernstian performance (57.66 , and 58.04 mV/pH, respectively) after 60 days.

By comparing the characteristics (chemical composition and surface morphology) of the 3 types of electrodes, it can be inferred that the different operation stability may be caused by the presence of surface nano-voids and the dissimilar percentage of PdO in the bulk. First, acid solutions containing chloride ions (from the filling solution of the reference electrode) may enter the nano-voids and react with the Pd in the bulk. The formation of chlorides of Pd gradually degrades the electrodes [51], hence reducing the amount of surface PdO and decreasing the sensitivity. XPS analysis was performed after the operation stability test for the electrode annealed at 250 °C for 48 h. The percentage of surface PdO reduced to $\sim 46\%$, indicating the degradation of the electrode surface. Second, the reactions between chloride ions and Pd are accompanied by the transferring of electrons. In the overall reaction, more electrons (m) than hydrogen ions (n) are transferred (i.e. $m > n$). Therefore, the sensitivity ($(n/m)(RT/F)$) becomes lower than 59.16 mV/pH at 25 °C. As a result, if a larger amount of metallic Pd is presented in the bulk of electrode, the electrode surface degrades faster and more electrons are transferred in the overall redox reaction. Both phenomena lead to a faster decreasing of sensitivity, which agrees with our observation. Moreover, other studies also found that the electrode aging may include dissolution and reaction of surface Pd when exposed to pH buffer solutions [11,21]. Thus, the operation stability could be improved by coating the electrode with a hydronium-permeable passivation material such as Nafion latex [18]. On the other hand, because of the similar chemical composition but different surface roughness of electrodes annealed at 200 °C and 250 °C for 48 h, it could be inferred that the surface roughness is not an important factor for the operation stability.

Storage stability is a measure of sensitivity degradation during storage before the first measurement. Since the electrode annealed at 200 °C for 48 h showed optimized performance in terms of sensitivity, response time, and operation stability, it was selected to study the storage stability. The electrode was kept in ambient

air at room temperature for 60 days before the first pH test. The resulting pH sensitivity after storage was 64.15 ± 1.85 mV/pH (5 measurement cycles), which was comparable with the sensitivity value of newly fabricated electrodes. This result demonstrated that the Pd/PdO sensing film has a minimum shelf-life of 60 days without any special care.

In addition, the electrode annealed at 200 °C for 48 h was continuously monitored in the pH=7 buffer solution for ~ 18 h. The drift rate of ~ 3.25 mV/h of this electrode was comparable with Pd/PdO pH sensing electrodes prepared from thermal oxidation [20,21]. As a consequence, we suggest the optimized process condition for the Pd/PdO pH sensing electrode was annealing at 200 °C for 48 h.

To study the reproducibility of the fabrication process and sensitivity of Pd/PdO electrodes, 7 electrodes were fabricated with annealing at 200 °C for 48 h. The sensitivity values of these electrodes were: 64.13 , 64.92 , 64.16 , 63.85 , 65.08 , 63.61 , and 64.71 mV/pH, with the average value of 64.35 mV/pH and standard deviation of 0.56 mV/pH. These consistent results demonstrated the fabrication process was reliable (or repeatable), and the performance of fabricated sensors was reproducible.

3.6. Perspectives of solution-processed Pd/PdO thin films

The reproducible and reliable sensing performance of the Pd/PdO thin films on glass substrate may have emerging potential for flexible sensors. The fabrication of sensing electrodes consumes a small amount of precursor and does not require high-temperature or vacuum equipment. So this process is simpler and cheaper than other approaches of fabricating Pd/PdO electrodes. Furthermore, the solution-based raw material could potentially be applied for ink-jet printing to make patterned structures for miniaturization. This could provide additional reduction of the cost because of the reduced material consumption. Moreover, the low annealing temperature provides the possibility to transfer this technology to flexible polymeric substrates such as polyimide which has glass transition temperatures in the range of 290 – 430 °C [28,52,53]. It is also worth noting that deposited Pd films showed good adhesion on polymer surfaces [54]. Therefore, the development of sensitive and low-cost pH sensors on flexible substrates is highly feasible.

4. Conclusions

Solution-processed Pd/PdO thin films were shown to be a promising pH-sensitive material. XPS, SEM, and AFM studies were used to determine the chemical composition and surface morphology of deposited Pd/PdO films. High sensitivity can be realized by forming more PdO at the electrode surface and in the bulk. Dense and flat surface morphology of the electrode can lead to a fast response. The presence of both metallic Pd and surface nano-voids in the electrodes causes to the decreasing of long-term sensitivity. pH sensing electrodes prepared by annealing Pd precursor solution at 200 °C for 48 h exhibited a linear super-Nernstian pH sensitivity of 64.71 ± 0.56 mV/pH in the pH range of 2–12 with a short response time less than 18 s, small hysteresis less than 7.81 mV, and high reproducibility with a standard deviation of 0.56 mV/pH of sensitivity. The super-Nernstian behavior may be related to the hydrous PdO_x ($x > 1$) produced from the solution-based process at low temperatures. A comparison of the fabrication processes and key performance parameters of Pd/PdO-based pH sensors reported in literature is listed in Table 2. Our proposed fabrication process uses solution-based material and does not require high temperature or vacuum equipment, which is compatible with large-area and low-cost manufacturing of high-performance pH sensors on flexible substrates. Future study will focus

Table 2
Comparison of the fabrication processes and key performance parameters of Pd/PdO-based pH sensors.

Sensor structure	Fabrication	Lowest processing temperature (°C)	Sensitivity (mV/pH) ^a	Sensing range (pH unit)	Response time (s)	Hysteresis (mV)	Drift rate (mV/h)	Lifetime	Ref.
Potentiometric	Solution processing	200	64.7 ± 0.6	2–12	< 18	< 7.81	3.25	> 60 days	This study
Potentiometric	Anodization	308	71.4 ± 5.2	3–9	0.5	–	–	6 days	[18]
Potentiometric	Anodization	308	60	3–9	2.5–5	–	–	< 14 days	[25]
Potentiometric	Anodization	23	55	3–11	< 2	–	–	> 21 days ^b	[26]
Potentiometric	Thermal oxidation	750	59.6	2.5–8	5–10	–	~3.5	–	[20, 22]
Potentiometric	Thermal oxidation	800	59.0 ± 1.2	3–11	–	–	–	6 years ^b	[19]
Potentiometric	Sputtering	50	54.5	3–9	–	–	–	–	[24]
Potentiometric	Sputtering	420	46	2–11	–	–	–	–	[16]
Extended-gate field-effect transistor	Evaporation+thermal oxidation	700	65.3 ± 2.1	2–12	–	7.9	2.32	6 test cycles	[21]

^a The standard deviation value in some studies were not given.

^b Stored in distilled water.

on the optimization of physical structures and process conditions for miniaturized all-printed pH sensors.

Acknowledgments

The authors are grateful to Sandra Gardner for the assistance in recording SEM images. This research is supported by Discovery Grants from the Natural Science and Engineering Research Council of Canada, an infrastructure grant from the Canada Foundation for Innovation, an Ontario Research Fund for Research Excellence Funding Grant, a FedDev of Southern Ontario grant, the Canada Research Chair program, NSERC ResEau strategic network and the NCE IC-IMPACTS.

Appendix A. Supplementary material

Supplementary data associated with this article can be found in the online version at <http://dx.doi.org/10.1016/j.talanta.2015.08.062>.

References

- [1] O. Korostynska, K. Arshak, E. Gill, A. Arshak, *IEEE Sens. J.* 8 (2008) 20–28.
- [2] M.H. Banna, S. Imran, A. Francisque, H. Najjaran, R. Sadiq, M. Rodriguez, M. Hoorfar, *Crit. Rev. Env. Sci. Technol.* 44 (2014) 1370–1421.
- [3] P. Kurzweil, *Sensors* 9 (2009) 4955–4985.
- [4] Y. Qin, H.J. Kwon, M. Howlader, M.J. Deen, *RSC Adv.* 5 (2015) 69086–69109.
- [5] S. Zaman, M.H. Asif, A. Zainelabdin, G. Amin, O. Nur, M. Willander, *J. Electroanal. Chem.* 662 (2011) 421–425.
- [6] H.-J. Chung, M.S. Sulkin, J.-S. Kim, C. Goudeseune, H.-Y. Chao, J.W. Song, S. Y. Yang, Y.-Y. Hsu, R. Ghaffari, I.R. Efimov, *Adv. Healthc. Mater.* 3 (2014) 59–68.
- [7] T.Y. Kim, S. Yang, *Sens. Actuators, B* 196 (2014) 31–38.
- [8] C.M. Nguyen, S. Rao, Y.-S. Seo, K. Schadt, Y. Hao, J.-C. Chiao, *IEEE Trans. Nanotechnol.* 13 (2014) 945–953.
- [9] J. Chu, Y. Zhao, S.-H. Li, H.-Q. Yu, G. Liu, Y.-C. Tian, *Electrochim. Acta* 152 (2015) 6–12.
- [10] M. Hussain, Z.H. Ibupoto, M.A. Abbasi, O. Nur, M. Willander, *J. Electroanal. Chem.* 717–718 (2014) 78–82.
- [11] L. Santos, J.P. Neto, A. Crespo, D. Nunes, N. Costa, I.M. Fonseca, P. Barquinha, L. Pereira, J. Silva, R. Martins, *ACS Appl. Mater. Interfaces* 6 (2014) 12226–12234.
- [12] A. Lale, A. Tsopela, A. Civélas, L. Salvagnac, J. Launay, P. Temple-Boyer, *Sens. Actuators, B* 206 (2015) 152–158.
- [13] A. Sardarinejad, D.K. Maurya, K. Alameh, *Sens. Actuators, A* 214 (2014) 15–19.
- [14] R. Zhao, M. Xu, J. Wang, G. Chen, *Electrochim. Acta* 55 (2010) 5647–5651.
- [15] S.M. Al-Hilli, M. Willander, A. Ost, P. Stralfoers, *J. Appl. Phys.* 102 (2007) 084304.
- [16] K.G. Kreider, M.J. Tarlov, J.P. Cline, *Sens. Actuators, B* 28 (1995) 167–172.
- [17] H. Arida, *Microchim. Acta* 181 (2014) 1–8.
- [18] C.-C. Liu, D.B. Bocchicchio, P.A. Overmyer, M.R. Neuman, *Science* 207 (1980) 188–189.
- [19] W.T. Grubb, L.H. King, *Anal. Chem.* 52 (1980) 270–273.
- [20] E. Kinoshita, F. Ingman, G. Edwall, S. Thulin, S. Glab, *Talanta* 33 (1986) 125–134.
- [21] A. Das, D.H. Ko, C.-H. Chen, L.-B. Chang, C.-S. Lai, F.-C. Chu, L. Chow, R.-M. Lin, *Sens. Actuators, B* 205 (2014) 199–205.
- [22] E. Kinoshita, F. Ingman, G. Edwall, S. Glab, *Electrochim. Acta* 31 (1986) 29–38.
- [23] C.-C. Liu, M.R. Neuman, *Diabetes Care* 5 (1982) 275–277.
- [24] V.A. Karagounis, C.C. Liu, M.R. Neuman, L.T. Romankiw, P.A. Leary, J.J. Cuomo, *IEEE Trans. Biomed. Eng.* (1986) 113–116.
- [25] J.Y. Kim, Y.H. Lee, *Biotechnol. Bioeng.* 34 (1989) 131–136.
- [26] L.J. Bloor, D.J. Malcolme-Lawes, *J. Electroanal. Chem. Interfacial Electrochem.* 278 (1990) 161–173.
- [27] Y. Qin, D.H. Turkenburg, I. Barbu, W.T.T. Smaal, K. Myny, W.-Y. Lin, G.H. Gelinck, P. Heremans, J. Liu, E.R. Meinders, *Adv. Funct. Mater.* 22 (2012) 1209–1214.
- [28] Y. Qin, M.M.R. Howlader, M.J. Deen, Y.M. Haddara, P.R. Selvaganapathy, *Sens. Actuators, B* 202 (2014) 758–778.
- [29] A. Santos, M.J. Deen, L.F. Marsal, *Nanotechnology* 26 (2015) 042001.
- [30] M.M.R. Howlader, P.R. Selvaganapathy, M.J. Deen, T. Suga, *IEEE J. Sel. Top. Quantum Electron.* 17 (2011) 689–703.
- [31] J.P. Metters, F. Tan, C.E. Banks, *J. Solid State Electrochem.* 17 (2013) 1553–1562.
- [32] C. Nguyen, W. Huang, S. Rao, H. Cao, U. Tata, M. Chiao, J.-C. Chiao, *IEEE Sens. J.* 13 (2013) 3857–3864.
- [33] P.-C. Yao, J.-L. Chiang, M.-C. Lee, *Solid State Sci.* 28 (2014) 47–54.
- [34] P.D. Batista, M. Mulato, *Appl. Phys. Lett.* 87 (2005) 143508.
- [35] M. Ren, Y. Kang, W. He, Z. Zou, X. Xue, D.L. Akins, H. Yang, S. Feng, *Appl. Catal., B* 104 (2011) 49–53.
- [36] D. Zemlyanov, B. Aszalos-Kiss, E. Kleimenov, D. Teschner, S. Zafeiratos, M. Hävecker, A. Knop-Gericke, R. Schlögl, H. Gabasch, W. Unterberger, *Surf. Sci.* 600 (2006) 983–994.
- [37] J. Hämäläinen, E. Puukilainen, T. Sajavaara, M. Ritala, M. Leskelä, *Thin Solid Films* 531 (2013) 243–250.
- [38] H. Wang, T. Sun, W. Xu, F. Xie, L. Ye, Y. Xiao, Y. Wang, J. Chen, J. Xu, *RSC Adv.* 4 (2014) 54729–54739.
- [39] M.W. Lee, G.S. Ryu, Y.U. Lee, C. Pearson, M.C. Petty, C.K. Song, *Microelectron. Eng.* 95 (2012) 1–4.
- [40] S. Glab, A. Hulanicki, G. Edwall, F. Ingman, *Crit. Rev. Anal. Chem.* 21 (1989) 29–47.
- [41] L.M. Vracar, D.B. Sepa, A. Damjanovic, *J. Electrochem. Soc.* 134 (1987) 1695–1697.
- [42] S.F. Parker, K. Refson, A.C. Hannon, E.R. Barney, S.J. Robertson, P. Albers, *J. Phys. Chem. C* 114 (2010) 14164–14172.
- [43] L.S. Kibis, A.I. Stadnichenko, S.V. Koscheev, V.I. Zaikovskii, A.I. Boronin, *J. Phys. Chem. C* 116 (2012) 19342–19348.
- [44] J. Park, M. Kim, S. Kim, *Sens. Actuators, B* 204 (2014) 197–202.
- [45] W.-D. Huang, H. Cao, S. Deb, M. Chiao, J.-C. Chiao, *Sens. Actuators, A* 169 (2011) 1–11.
- [46] L. Bousse, S. Mostarshed, B. van der Schoot, N.F. De Rooij, *Sens. Actuators, B* 17 (1994) 157–164.
- [47] M.W. Shinwari, M.J. Deen, D. Landheer, *Microelectron. Reliab.* 47 (2007) 2025–2057.
- [48] M.W. Shinwari, D. Zhitomirsky, I.A. Deen, P.R. Selvaganapathy, M.J. Deen, D. Landheer, *Sens. Actuators, B* 10 (2010) 1679–1715.
- [49] M.J. Deen, B. Iñiguez, O. Marinov, F. Lime, *J. Mater. Sci. – Mater. Electron.* 17 (2006) 663–683.
- [50] M.J. Deen, F. Pascal, *J. Mater. Sci. – Mater. Electron.* 17 (2006) 549–575.
- [51] S. Chen, W. Huang, J. Zheng, Z. Li, *J. Electroanal. Chem.* 660 (2011) 80–84.
- [52] M.M.R. Howlader, T.E. Doyle, S. Mohtashami, J.R. Kish, *Sens. Actuators, B* 178 (2013) 132–139.
- [53] M.M.R. Howlader, A.U. Alam, R.P. Sharma, M.J. Deen, *PCCP* 17 (2015) 10135–10145.
- [54] L. Ravagnan, G. Divitini, S. Rebasti, M. Marelli, P. Piseri, P. Milani, *J. Phys. D: Appl. Phys.* 42 (2009) 082002.